Results in Physics 6 (2016) 481–495

Contents lists available at ScienceDirect

Results in Physics

journal homepage: www.journals.elsevier.com/results-in-physics

Effects of thermal-diffusion and viscous dissipation on peristaltic flow of micropolar non-Newtonian nanofluid: Application of homotopy perturbation method

Mohamed Abou-zeid *

Department of Mathematics, Faculty of Education, Ain Shams University, Heliopolis, Roxy, Cairo 11757, Egypt
Department of Mathematics, Faculty of Science, University of Tabuk, Tabuk 71491, Saudi Arabia

ARTICLE INFO

Article history:
Received 19 May 2016
Accepted 5 August 2016
Available online 12 August 2016

Keywords:
Peristaltic flow
Nanofluid
Micropolar fluid
Homotopy perturbation method

ABSTRACT

In this paper, a study of the peristaltic motion of incompressible micropolar non-Newtonian nanofluid with heat transfer in a two-dimensional asymmetric channel is investigated under long-wavelength assumption. The flow includes radiation and viscous dissipation effects as well as all micropolar fluid parameters. The fundamental equations which govern this flow have been modeled under long-wavelength assumption, and the expressions of velocity and microrotation velocity are obtained in a closed form, while the solutions of both temperature and nanoparticles phenomena are obtained using the homotopy perturbation method (HPM). Also, the skin friction, Nusselt number and Sherwood number are obtained at both lower and upper walls. The results have been discussed graphically to observe the effects the physical parameters of the problem have on the physical quantities.

Introduction

An auxiliary or less consistent diffusion of incompliant particles among intentional teeny diameters in nanometers is called nanofluid. Recently, the study of transport with heat transfer of nanofluids has gained great importance due to its applications such as industrial cooling applications, smart fluids, nuclear reactors, nanofluid coolant, nanofluid in fuel, cooling of microchips, microscale fluidic applications, cancer therapeutics, and nanocryosurgery. Brownian motion balances these particles which are dispersed in a balance between optimistic mass and thermal campaigning when they are in symmetry with no flow [1]. Estellé et al. [2] report experimental results on the steady state rheological behavior of carbon nanotubes. A number of studies related to the effect of mechanical methods on the viscosity of nanofluids have been presented. Saeed et al. [3] investigated numerically the problem of laminar flow-forced convective heat transfer of nanofluids in a triangular duct under constant wall temperature condition. The peristaltic transport of nanofluids involving the combined effects of Brownian motion and thermophoretic diffusion of nanoparticles in a channel with complaint walls is studied by Mustafa et al. [4]. Umavathi and Shekar [5] analyzed the problem of Jeffery-Hamel flow of nanofluid with magnetic effect. Khan et al. [6] studied the unsteady free convection boundary-layer flow of a nanofluid along a stretching sheet with thermal radiation in the presence of magnetic field.

Fluids which consist of rigid, randomly oriented (or spherical) particles suspended in a viscous medium are called micropolar fluids, where the deformation of the particles is ignored. Eringen [7] developed the theory of thermo-micropolar fluids. Micropolar fluids are considered to be the model of blood flow in small arteries [8]. Nadeem et al. [9] carried out the axisymmetric stagnation flow of a micropolar nanofluid in a moving cylinder with finite radius. The effects of viscoelastic wall properties and micropolar fluid parameters on the peristaltic flow of an incompressible micropolar fluid are carried by Muthu et al. [10]. Ali and Hayat [11] compared the results of micropolar fluids with those of Newtonian fluids for the peristaltic motion of an incompressible fluid in an asymmetric channel. The micropolar fluid flow through an isotropic porous medium with heat transfer characteristics in a two-dimensional channel with rhythmically contracting walls is discussed by Abd Elmaboud [12].

It is well known that many physiological fluids behave in general like suspensions of deformable or rigid particles in a Newtonian fluid. Blood, for example, is a suspension of red cells, white cells and platelets in plasma. Another example is cervical mucus,

* Address: Department of Mathematics, Faculty of Education, Ain Shams University, Heliopolis, Roxy, Cairo 11757, Egypt.
E-mail address: master_math2003@yahoo.com

http://dx.doi.org/10.1016/j.rinp.2016.08.006
2211-3797/

which is a suspension of macromolecules in a water-like liquid. In view of this, some researchers have tried to account for the suspension behavior of biofluids by considering them non-Newtonian [13]. Eldabe and Abou-zeid [14] studied the problem of the unsteady peristaltic mechanism with heat and mass transfer of an incompressible micropolar non-Newtonian fluid in a two-dimensional channel. The flow includes the viscoelastic wall properties, micropolar fluid parameters as well as the viscous dissipation effect. Dissipation is the process of converting the mechanical energy of downward-flowing water into thermal and acoustical energy. The steady two-dimensional convective micropolar boundary layer driven by a pseudoplastic power-law fluid on a vertical plate is reported by Ferdows and Olajuwon [15]. Wang [16] considered a motion of an incompressible non-Newtonian magneto-micropolar fluid. He assumed that the stress tensor has a *p*-structure. Ellahi et al. [17] presented the unsteady and incompressible flow of non-Newtonian fluid through composite stenosis. Micropolar fluids are treated as a blood flow model. A study on boundary layer flow of a nanofluid through a porous medium subjected to a magnetic field, thermal radiation, viscous dissipation and chemical reaction effects is explained by Haile and Shankar [18]. The effects of porosity, thermal radiation, magnetic field, viscous dissipation and chemical reaction to the flow field were taken into their consideration.

Mehmood et al. [19] carried out a study of heat and mass transfer effects on non-linear peristaltic transport of Walter's B fluid in an asymmetric channel. The governing equations are solved using the regular perturbation method. Micropolar, nanofluid and radiation effects weren't taken into their consideration. Due to their importance with respect to many researchers in the last decade, in this study, the heat transfer of peristaltic motion of a micropolar non-Newtonian biviscosity nanofluid is treated analytically. Also, the viscous dissipation and radiation effects are taken into consideration. The closed form for the velocity and microrotation velocity are presented, while homotopy perturbation method (HPM) is used to obtain analytic approximate solution for the temperature and nanoparticle profiles. The results have been discussed to observe the effects of non-Newtonian, micropolar, viscous dissipation, nanofluid, radiation parameters and Reynolds number, on the physical quantities of the problem through a set of figures.

Formulation of the problem

Consider a two-dimensional peristaltic pump of an incompressible micropolar biviscosity nanofluid in an asymmetric channel, with heat transfer. The flow is generated by sinusoidal waves propagating which are of different amplitudes a_1, a_2 at lower and upper walls, respectively, of difference phases θ and constant speed $\bar{c}$ along the channel walls (see Fig. 1). The lower and upper walls are at distance b_1 and b_2 from the centerline ($Y = 0$) of the channel.

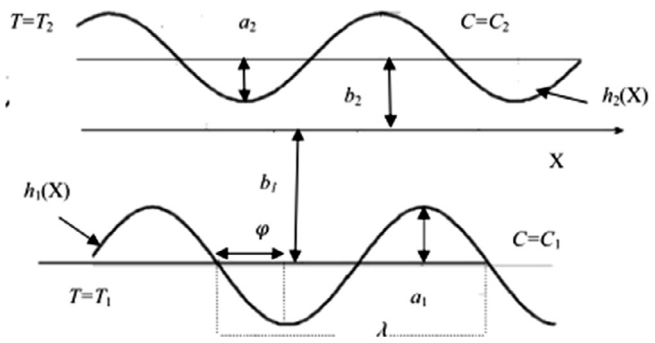

Fig. 1. Geometry of two-dimensional asymmetric channel.

A rectangular coordinate system is chosen such that the axes X and Y are in the directions of wave propagation and normal to the mean position of the wave respectively. The lower wall is kept at temperature T_1 and nanoparticle phenomena f_1, while the upper wall is kept at temperature T_2 and nanoparticle phenomena f_2. The limiting process by which the biviscosity model is approached with the limiting process is implicit in the lubrication theory [20]. Models of this type are much easier to handle mathematically than many models and represent the experimental facts just as well, at least in many cases [14].

The biviscosity model [13] can be written as

$$\tau_{ij} = \begin{cases} 2\left(\mu_B + p_y/\sqrt{2\pi}\right)e_{ij}, & pi \geqslant \pi_c \\ 2\left(\mu_B + p_y/\sqrt{2\pi}\right)e_{ij} & ,\pi < \pi_c \end{cases}. \tag{1}$$

The following quantity is introduced as a non-dimensional parameter including π_c

$$\alpha = \mu_B\sqrt{2\pi_c}/p_y,$$

where μ_B is the plastic viscosity, p_y is the yielding stress, $\pi = e_{ij}\, e_{ij}$, where e_{ij} is the (i,j) component of the deformation rate and the value of α denotes the upper limit of apparent viscosity coefficient. The biviscosity model is approached in the limit $\alpha \to \infty$ (see Eldabe and Abou-zeid [13] for a few further details).

The governing continuity, momentum, angular momentum, temperature and concentration equations for this problem can be written as follows:

$$\frac{\partial U}{\partial X} + \frac{\partial V}{\partial Y} = 0, \tag{2}$$

$$\rho_f\left[\frac{\partial U}{\partial t} + U\frac{\partial U}{\partial X} + V\frac{\partial U}{\partial Y}\right] = -\frac{\partial P}{\partial X} + \left(\frac{2\mu_B(1+\alpha^{-1}) + k_1}{2}\right)\nabla^2 U + k_1\frac{\partial N_\theta}{\partial Y}, \tag{3}$$

$$\rho_f\left[\frac{\partial V}{\partial t} + U\frac{\partial V}{\partial X} + V\frac{\partial V}{\partial Y}\right] = -\frac{\partial P}{\partial Y} + \left(\frac{2\mu_B(1+\alpha^{-1}) + k_1}{2}\right)\nabla^2 V - k_1\frac{\partial N_\theta}{\partial X}, \tag{4}$$

$$\rho_f J\left[\frac{\partial N}{\partial t} + U\frac{\partial N}{\partial X} + V\frac{\partial N}{\partial Y}\right] = -2k_1 N + \bar{\gamma}\nabla^2 N + k_1\left[\frac{\partial V}{\partial X} - \frac{\partial U}{\partial Y}\right], \tag{5}$$

$$\begin{aligned}(\rho c)_f\left[\frac{\partial T}{\partial t} + U\frac{\partial T}{\partial X} + V\frac{\partial T}{\partial Y}\right] &= k_c\nabla^2 T + \left(\frac{2\mu_B,(1+\alpha^{-1}) + k_1}{2}\right) \\ &\times\left[2\left(\frac{\partial U}{\partial X}\right)^2 + 2\left(\frac{\partial V}{\partial Y}\right)^2 + \left(\frac{\partial U}{\partial Y} + \frac{\partial V}{\partial X}\right)^2\right] \\ &+ 2k_1\left[N^2 - N\left(\frac{\partial V}{\partial X} - \frac{\partial U}{\partial Y}\right)\right] \\ &+ \bar{\gamma}\left[\left(\frac{\partial N}{\partial X}\right)^2 + \left(\frac{\partial N}{\partial Y}\right)^2\right] - \frac{\partial q}{\partial y} \\ &+ (\rho c)_p\left[D_B\left(\frac{\partial T}{\partial X}\frac{\partial f}{\partial X} + \frac{\partial T}{\partial Y}\frac{\partial f}{\partial Y}\right)\right. \\ &\left.+ \frac{D_T}{T_1}\left(\left(\frac{\partial T}{\partial X}\right)^2 + \left(\frac{\partial T}{\partial Y}\right)^2\right)\right],\end{aligned} \tag{6}$$

$$\frac{\partial f}{\partial t} + U\frac{\partial f}{\partial X} + V\frac{\partial f}{\partial Y} = D_B\left(\frac{\partial^2 f}{\partial X^2} + \frac{\partial^2 f}{\partial Y^2}\right) + \frac{D_T k_T}{T_1}\left(\frac{\partial^2 T}{\partial X^2} + \frac{\partial^2 T}{\partial Y^2}\right), \tag{7}$$

with the boundary:

$$U=0,\quad V=0,\quad N=0,\quad T=T_1,\quad f=f_1\quad at\quad y=h_1, \tag{8}$$

$$U=0,\quad V=0,\quad N=0,\quad T=T_2,\quad f=f_2\quad at\quad y=h_2, \tag{9}$$

$$h_1=-b_1-a_1\sin\frac{2\pi}{\lambda}[(X-\bar{c}t)+\theta], \tag{10}$$

$$h_2=1.5b_2+a_2\sin\frac{2\pi}{\lambda}(X-\bar{c}t), \tag{11}$$

where $U(X, Y, t)$ and $V(X, Y, t)$ are the velocity components in the X and Y directions respectively, $N(X, Y, t)$ is the microrotation velocity component in the direction normal to both the X and Y axis. ρ_f and ρ_p are the densities of fluid and particle respectively, P is the pressure, t is the time, J is the microinertia constant, k_1 is the vortex viscosity coefficient, $\bar{\gamma}$ is the spin-gradient viscosity. The fluid temperature and nanoparticles phenomena are $T(X, Y, t)$ and $f(X, Y, t)$, c is the volumetric volume expansion, $(\rho c)_f$ and $(\rho c)_p$ are heat capacity of the fluid and effective heat capacity of the nanoparticle material respectively, D_B is Brownian diffusion coefficient and D_T is the thermophoretic diffusion coefficient, K_T is the thermal diffusion ratio, k_c the thermal conductivity, q is the radiative heat flux and λ is the wave length. The last term in Eq. (7) refers the influence of thermal-diffusion. Further, the following inequalities are satisfied [7]:

$$2\mu_B+k_1\geqslant 0,\quad k_1\geqslant 0,\quad \mu_B\geqslant 0. \tag{12}$$

Eq. (2) allows the use of the stream function $\psi(X, Y, t)$ such that

$$U=\frac{\partial\psi}{\partial Y}\quad\text{and}\quad V=-\frac{\partial\psi}{\partial X}. \tag{13}$$

However, if observed in a coordinate system (X, Y) moving with constant speed, it can be treated as steady because the boundary shape appears to be stationary.

The transformation between the two frames is given by

$$x=X-\bar{c}t,\quad y=Y,\quad u=U-\bar{c},\quad v=V, \tag{14}$$

By using the Rosseland approximation [22], the radiative heat flux is given by

$$q=\frac{-4\sigma^*}{3k_R}\frac{\partial T^4}{\partial y}, \tag{15}$$

where σ^* is the Stefan Boltzmann constant and k_R is the mean absorption coefficient. We assume that the temperature differences within the flow are sufficiently small such that T^4 may be expressed as a linear function of temperature. This is accomplished by expanding T^4 in a Taylor series about T_1 and neglecting higher-order terms, one gets

$$T^4\approx 4T_1^3T-3T_1^4. \tag{16}$$

By introducing the following non-dimensional quantities:

$$x^*=\frac{x}{\lambda},\quad y^*=\frac{y}{b_2},\quad u^*=\frac{u}{\bar{c}},\quad v^*=\frac{v}{\bar{c}},\quad P^*=\frac{b_2^2}{\lambda\bar{c}\mu_B}P,\quad N^*=\frac{b_2}{\bar{c}}N,$$
$$T^*=\frac{T-T_1}{T_2-T_1},\quad f^*=\frac{f-f_1}{f_2-f_1},\quad j^*=\frac{j}{b_2^2},\quad h_1^*=\frac{h_1}{b_2},\quad h_2^*=\frac{h_2}{b_2},\quad \delta=\frac{b_2}{\lambda}, \tag{17}$$

Substituting from Eq. (17) into Eqs. (2)–(7), after applying the long-wavelength approximation to our analysis as described in Ref. [13], and dropping the star mark for simplicity, then the governing equations may be written as

$$\frac{\partial P}{\partial x}=\left[(1+\alpha^{-1})+\beta\right]\frac{\partial^3\psi}{\partial y^3}+\beta,\frac{\partial N}{\partial y}, \tag{18}$$

$$\frac{\partial P}{\partial y}=0, \tag{19}$$

$$2\beta N+\beta\frac{\partial^2\psi}{\partial y^2}-\gamma\frac{\partial^2 N}{\partial y^2}=0, \tag{20}$$

$$\left(1+\frac{4}{3}R\right)\frac{\partial^2 T}{\partial y^2}+\frac{2Ec\Pr}{\mathrm{Re}}(1+\alpha^{-1})\left(\frac{\partial^2\psi}{\partial y^2}\right)^2+N_b\left(\frac{\partial T}{\partial y}\frac{\partial f}{\partial y}\right)+N_t\left(\frac{\partial T}{\partial y}\right)^2+\frac{2\beta Ec}{\mathrm{Re}}\left(N^2+N\frac{\partial^2\psi}{\partial y^2}\right)=0, \tag{21}$$

$$\frac{\partial^2 f}{\partial y^2}+\frac{N_t}{N_b}\left(\frac{\partial^2 T}{\partial y^2}\right)=0. \tag{22}$$

where the dimensionless parameters are defined by:

$\mathrm{Re}=\frac{\rho\bar{c}b_2}{\mu_B}$	(Reynolds number),
$\gamma=\frac{\bar{\gamma}}{\mu_B b_2^2}$	(the microrotation parameter),
$Ec=\frac{\bar{c}^2}{c_f(T_2-T_1)}$	(Eckert number),
$N_t=\frac{D_T(T_2-T_1)(\rho c)_p}{T_1(\rho c)_f\bar{c}b_2}$	(the thermophoresis parameter),
$\beta=\frac{k_1}{\mu_B}$	(the dimensionless viscosity ratio),
$\Pr=\frac{(\rho c)_f\bar{c}b_2}{k_c}$	(Prandtl number),
$R=\frac{4\sigma^*T_1^3}{kk_R}$	(the radiation parameter),
$N_b=\frac{D_B(C_2-C_1)(\rho c)_p}{(\rho c)_f\bar{c}b_2}$	(Brownian motion parameter).

In the moving frame, the adherence boundary conditions (8) and (9) can be rewritten in dimensionless form, as

$$\frac{\partial^2\psi}{\partial y^2}=-1,\quad N=0,\quad T=0,\quad f=0\quad\text{at}\quad y=h_1$$
$$=-b-a\sin[2\pi,x+\theta]. \tag{23}$$

$$\frac{\partial^2\psi}{\partial y^2}=-1,\quad N=0,\quad T=1,\quad f=1\quad\text{at}\quad y=h_2$$
$$=1.5+d\sin 2\pi x. \tag{24}$$

If $(\alpha\to\infty,\beta=0,\gamma=0,N_b=0,N_t=0)$, this work tends to the work of Mehmood et al. [19] in the case of zeroth order.

Eliminating the pressure gradient between (18) and (19) we get

$$0=\left[(1+\alpha^{-1})+\beta\right]\frac{\partial^4\psi}{\partial y^4}+\beta\frac{\partial^2 N}{\partial y^2}. \tag{25}$$

Because Eq. (25) is a fourth-order differential equation for ψ in y, in addition to the two adherence boundary conditions in (23) and (24) for ψ, two additional boundary conditions are needed, we do this by choosing the zero value of the stream function at the wall ($y=0$) [24] and from Beavers-Joseph boundary conditions for non-Newtonian fluid, u is maximum on the middle line [25], thus choosing $\frac{\partial^2\psi}{\partial y^2}=0$ at $y=\frac{h_1+h_2}{2}$.

Method of solution

The closed solutions for the stream function $\psi(x,y)$, and the microrotation velocity $N(x, y)$ are given by

$$\psi(x,y)=a_{14}e^{-\sqrt{a_1}y}+a_{13}e^{\sqrt{a_1}y}+a_{11}y^2+a_{12}y^3+a_{15}y+a_{16}, \tag{26}$$

$$N(x,y)=a_7e^{-\sqrt{a_1}y}+a_6e^{\sqrt{a_1}y}-\frac{a_3+a_2y}{a_1}, \tag{27}$$

where a_1–a_{21}, are given in the Appendix A.

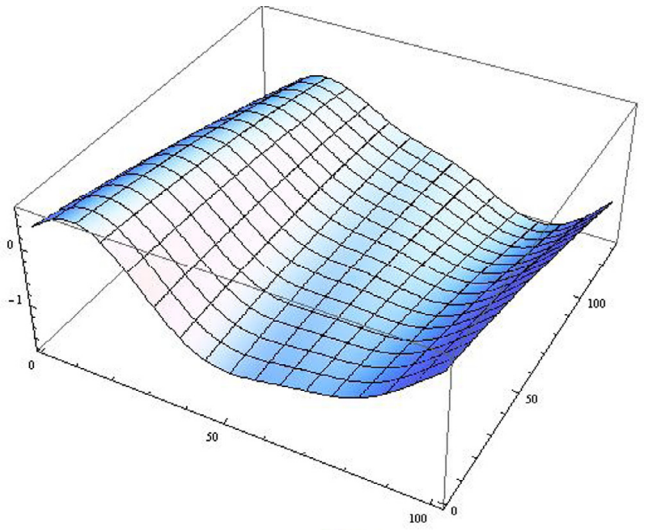

Fig. 2. Three-dimensional velocity is plotted versus y and x for a system having the particulars $\alpha = 1.2$, $Ec = 3$, $\gamma = 2$, $\frac{dp}{dx} = -1$, Pr = 1, Re = 0.01, $N_b = 0.5$, $N_t = 1.5$, $R = 1$, $d = 0.8$, $a = 2$, $b = 1.8$, and $\theta = \pi/2$. The figure indicates the relation (26).

The homotopy perturbation method (HPM), preserves all advantages of traditional perturbation methods, and removes its drawbacks, since it is a combination of the perturbation method and the homotopy method. So, the homotopy perturbation method [26] is used to solve Eqs. (21) and (22) as follows:

$$H(p,T) = (1-p)[L(T) - L(T_{10})] + p\left(L(T) + \frac{3}{3+4R}\left[\frac{2Ec\,\mathrm{Pr}}{\mathrm{Re}}(1+\alpha^{-1})\left(\frac{\partial^2\psi}{\partial y^2}\right)^2 + N_b\left(\frac{\partial T}{\partial y}\frac{\partial f}{\partial y}\right) + N_t\left(\frac{\partial T}{\partial y}\right)^2 + \frac{2\beta Ec}{\mathrm{Re}}(N^2 + N\frac{\partial^2\psi}{\partial y^2})\right]\right) \quad (28)$$

$$H(p,f) = (1-p)[L(f) - L(f_{10})] + p\left(L(f) + \frac{N_t}{N_b}\frac{\partial^2 T}{\partial y^2}\right), \quad (29)$$

where $L = \frac{\partial^2}{\partial y^2}$ is the linear operator, the initial approximations T_{10} and f_{10} can be defined as

$$T_{10}(x,y) = f_{10}(x,y) = \frac{y-h_1}{h_2-h_1}, \quad (30)$$

and assuming that:

$$T(y,p) = T_0 + pT_1 + p^2T_2 + \cdots, \quad (31)$$

$$f(y,p) = f_0 + pf_1 + p^2f_2 + \cdots \quad (32)$$

The solution of temperature and nanoparticles phenomenon (for $p = 1$) are obtained as follows:

$$T(x,y) = \frac{y-h_1}{h_2-h_1} + a_{35}e^{-2\sqrt{a_1}y} + (a_{36}+a_{37}y)e^{-\sqrt{a_1}y} + (a_{38}+a_{45}y)e^{\sqrt{a_1}y} + a_{46}e^{2\sqrt{a_1}y} + a_{55}y^5 + a_{50}y^4 + a_{56}y^3 + a_{57}y^2 + a_{58}y + a_{59}, \quad (33)$$

$$f(x,y) = \frac{y-h_1}{h_2-h_1} - \frac{N_t}{N_b}(a_{22}e^{-2\sqrt{a_1}y} + (a_{23}+a_{24}y)e^{-\sqrt{a_1}y} + (a_{27}+a_{28}y)e^{\sqrt{a_1}y} + a_{31}e^{2\sqrt{a_1}y} + a_{34}y^4 + a_{33}y^3 + a_{32}y^2 + a_{40}y + a_{39}), \quad (34)$$

where a_{22}–a_{61} are given in the appendix.

Now, the skin friction coefficient τ_{xy}, the heat transfer coefficient (Nusselt number) Nu and Sherwood number Sh at both lower and upper walls of the tube, are defined, respectively, by

$$\tau_\omega = \left[((1+\alpha^{-1})+\beta)\frac{\partial^2\psi}{\partial y^2} + \beta N\right]_{y=h_1,h_2}, \quad Nu = \left.\frac{\partial T}{\partial y}\right|_{y=h_1,h_2}, \quad Sh = \left.\frac{\partial f}{\partial y}\right|_{y=h_1,h_2}. \quad (35)$$

These expressions are evaluated by substituting from Eqs. (26), (33) and (34) into Eq. (35) respectively, and they have been evaluated numerically for several values of the parameters of the problem, using the software Mathematica package. The next section will discuss the obtained results.

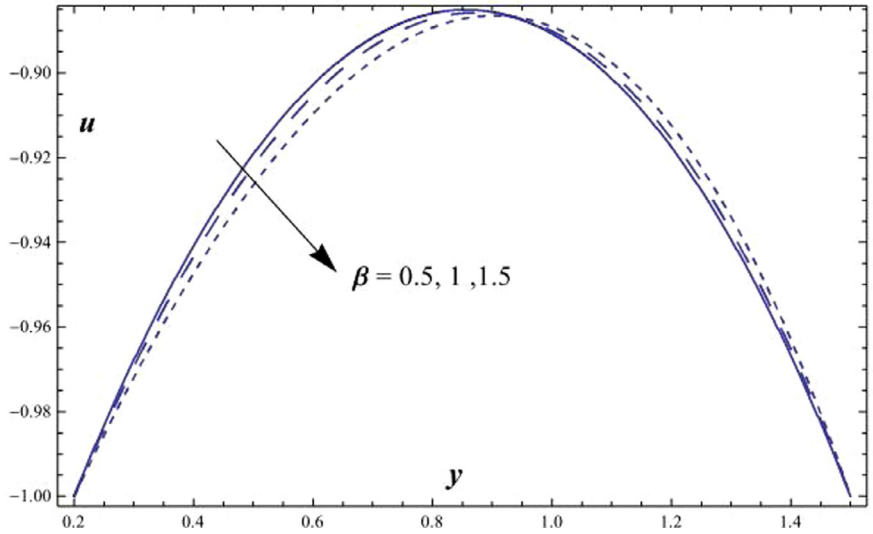

Fig. 3. The variation of velocity distribution versus y, with fixed $\alpha = 1.2$, $Ec = 3$, $\gamma = 2$, $\frac{dp}{dx} = -1$, Pr = 1, Re = 0.01, $N_b = 0.5$, $N_t = 1.5$, $R = 1$, $d = 0.8$, $a = 2$, $b = 1.8$, $\theta = \pi/2$, $x = 0.5$ for various values of β.

Results and discussion

In order to analyze the influence of the parameters of non-Newtonian fluid, nanofluid and heat transfer on the solutions of the considered problem, numerical computations are calculated from formulae (26), (27), (33) and (34) for the velocity $u(x, y)$, temperature $T(x, y)$, nanoparticles phenomena $f(x, y)$. The following values have been used by Mehmood et al. [19]

$$d = 0.8;\ a = 2;\ b = 1.8;\ \theta = \pi/2;\ x = 0.5;$$

A three-dimensional diagram is drawn to illustrate the effects of horizontal coordinate x and vertical coordinate y on the velocity u in Fig. 2, it is observed from this figure that the velocity u decreases with increasing x near the lower and upper walls, otherwise it increases, while it increases as y increases till a maximum value, and then it decreases till a minimum value.

Figs. 3 and 4 clarify the changes of the velocity u versus the normal axis to wave propagation y for different values of the dimensionless viscosity ratio β and the microrotation parameter γ. The relative strengths of the vortex viscosity coefficient to the viscosity coefficient is measured by the ratio k/μ_B, while the ratio $\bar{\gamma}/\mu_B$ measures the spin gradient viscosity coefficient to the viscosity coefficient. These coefficients μ_B, k and γ are always greater than or equal to zero. For example, the blood 50% hematocrit has the values $\mu_B = 0.0029$, $k = 0.000232$ and $\bar{\gamma} = 0.000001$ [13]. As the vortex viscosity coefficient effects are much smaller than the viscosity coefficient effects, the ratio k/μ_B tends to zero the size of the microstructure is signified by the microrotation parameter γ, and for a given small (large) value of γ is related to small (large) size of the particles [21]. It is observed from Fig. 2, that the velocity decreases with the increasing of β near the lower wall, while it increases as β increases when $y \geqslant 0.9$. Also, Fig. 4 shows that the velocity increases as γ increases but at $y > 1$, an opposite effect is noticed near the upper wall. The results in our study are consistent with those which are obtained by Eldabe and Abouzeid [14] in the case of isothermal wall. When the upper limit of apparent viscosity

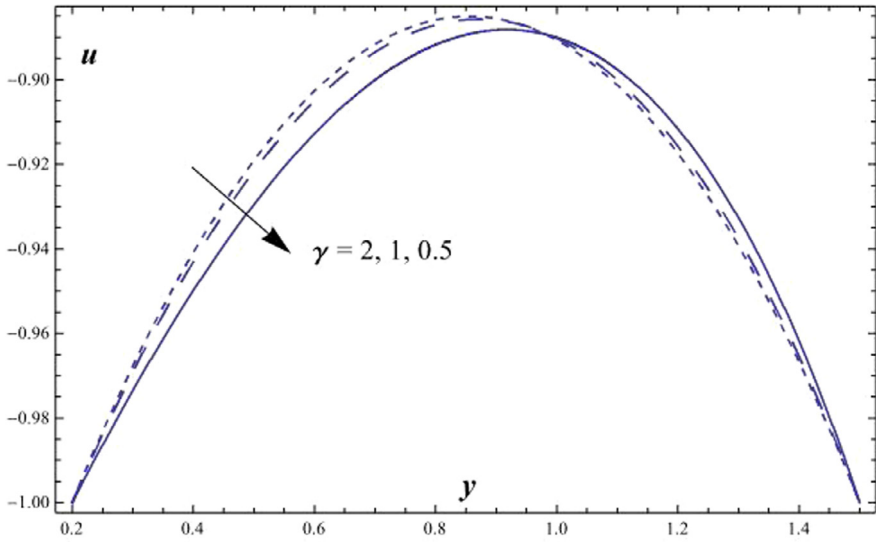

Fig. 4. The variation of velocity distribution versus y, with fixed $\beta = 0.5$, $\alpha = 1.2$, $Ec = 3$, $\frac{dP}{dx} = -1$, Pr = 1, Re = 0.01, $N_b = 0.5$, $N_t = 1.5$, $R = 1$, $d = 0.8$, $a = 2$, $b = 1.8$, $\theta = \pi/2$, $x = 0.5$ for various values of γ.

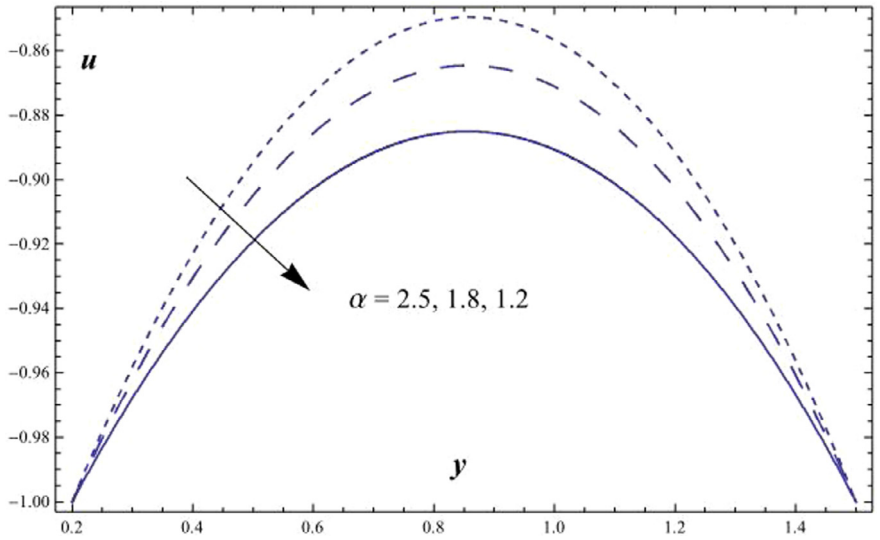

Fig. 5. The variation of velocity distribution versus y, with fixed $\beta = 0.5$, $Ec = 3$, $\gamma = 2$, $\frac{dP}{dx} = -1$, Pr = 1, Re = 0.01, $N_b = 0.5$, $N_t = 1.5$, $R = 1$, $d = 0.8$, $a = 2$, $b = 1.8$, $\theta = \pi/2$, $x = 0.5$ for various values of α.

coefficient $\alpha \to \infty$, the fluid is treated as Newtonian fluid. In Fig. 5, we see the effect of α on the velocity u. It is seen, from Fig. 5, that the velocity increases with the increase of α . It is also noted that the difference of the velocity for different values of α becomes greater with increasing the normal axis y and reaches maximum value after which it decreases. Note that the maximum value of u increases by increasing α,and this also occurs at another value $y > y_0$. The effects of the pressure gradient $\frac{dP}{dx}$ on the velocity is found to be exactly similar to the effect of α given in Fig. 5.

The effects of both the microrotation parameter γ, and the upper limit of apparent viscosity coefficient α on the microrotation N is shown in Figs. 6 and 7, respectively, and it is clear that the microrotation is always negative, and it increases by increasing γ, while it decreases with the increase of α. Also, it is noted that N decreases as y increases till a minimum value, after which N increases. if we draw the variation of N with y for different values of the dimensionless viscosity ratio β, we will obtain a figure in which the behavior of the curves are the same as that obtained in Fig. 7, except that the obtained curves are very close to those obtained in Fig. 7.

Figs. 8 and 9 show the variations of the temperature distribution T versus the normal coordinate y with several values of Eckert number Ec and the thermophoresis parameter N_t, respectively. It is seen, from Figs. 8 and 9, that the temperature increases with the increase of Ec, whereas it decreases as N_t increases. It is also noted that the difference of the temperature for different values of Ec and N_t becomes greater with increasing the normal coordinate y and reaches the maximum value after which it decreases. Note that the maximum value of T increases by increasing Ec and N_t, and this also occurs at another value $y > y_0$. The results in Fig. 8 are in a good agreement with physical expectations; since the temperature of source and dissipation effects always increase the energy transport rate of the fluid and accordingly the fluid temperature. Also, the effect of viscous dissipation on the temperature distribution, in case of non-Newtonian fluid, has been studied by Eldabe and Abouzeid [13]. The results in Fig. 8, are in agreement with those

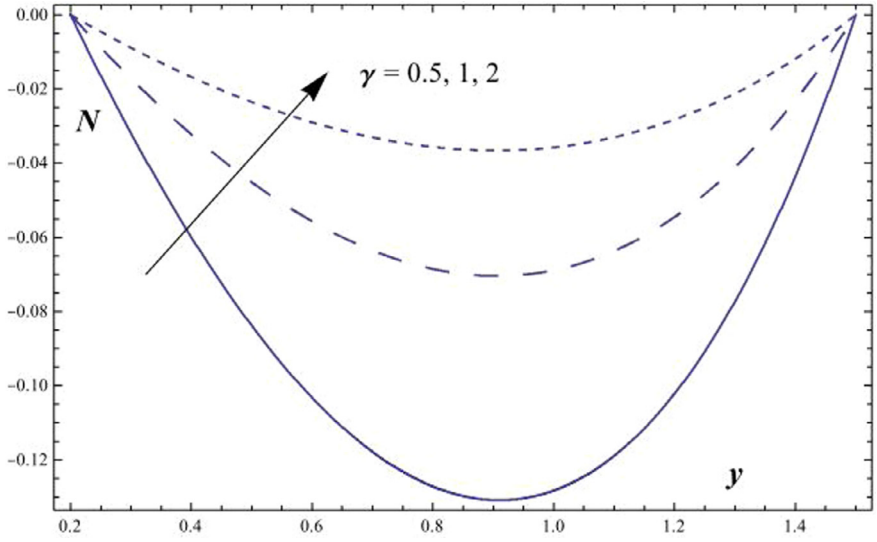

Fig. 6. The variation of microrotation velocity distribution versus y, with fixed $\beta = 0.5$, $\alpha = 1.2$, $Ec = 3$, $\frac{dP}{dx} = -1$, Pr = 1, Re = 0.01, $N_b = 0.5$, $N_t = 1.5$, $R = 1$, $d = 0.8$, $a = 2$, $b = 1.8$, $\theta = \pi/2$, $x = 0.5$ for various values of γ.

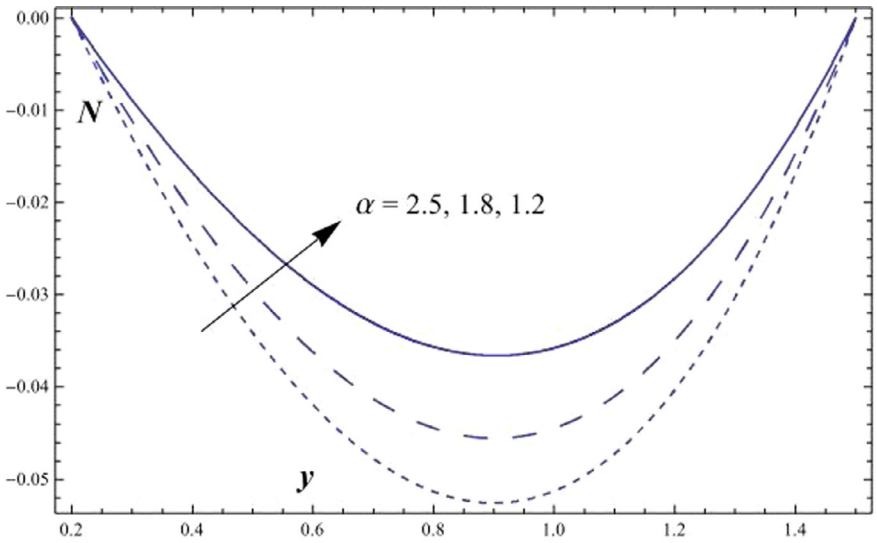

Fig. 7. The variation of microrotation distribution versus y, with fixed $\beta = 0.5$, $Ec = 3$, $\gamma = 2$, $\frac{dP}{dx} = -1$, Pr = 1, Re = 0.01, $N_b = 0.5$, $N_t = 1.5$, $R = 1$, $d = 0.8$, $a = 2$, $b = 1.8$, $\theta = \pi/2$, $x = 0.5$ for various values of α.

obtained by Eldabe and Abouzeid [13]. The effect of Prandtl number Pr on T is found to be similar to the effect of Ec on T shown in Fig. 8, while opposite qualitative behavior for the effect of Ec on T is shown in Fig. 8 in the case of study of the effects of Reynolds number, radiation parameter and Brownian motion parameter N_b on T; their figures are excluded here to save space. The behavior of the temperature distribution T with the normal axis y for various values of the dimensionless viscosity ratio β is depicted in Fig. 10. It is clear, from Fig. 10, that the effect of β on the temperature can be neglected near the lower and upper walls and the temperature increase as y increases till a maximum value, after which it decreases. When $0.2 < y < 0.7$, the temperature decreases with the increase of β, but at $y > 0.7$, an increase in β leads to increase the temperature distribution. In Fig. 11, the temperature T is plotted versus the coordinate y for various values of the microrotation parameter γ . It is clear that the effect of γ on T will behave in an opposite manner to the effect of β on T that is given in Fig. 11. Also, it is found that all obtained curves intersect at $y = 0.55$.

It is interesting to note that Brownian motion parameter of nanoparticles, at molecular and nanoscale levels, is a key nanoscale mechanism governing their thermal behaviors. In nanofluid systems, due to the size of nanoparticles, Brownian motion parameter takes place, which can affect the heat transfer properties [23]. Figs. 12 and 13 represent the behaviors of the nanoparticles phenomena f with the dimensionless normal coordinate y for different values of Brownian motion parameter N_b and Prandtl number Pr, respectively. It is observed from Figs. 12 and 13, that the nanoparticles phenomena f increases with the increase of N_b, whereas it decreases as Pr increases, respectively. It is also noted that the difference of the nanoparticles phenomena f for different values of N_b and Pr becomes greater with increasing the normal coordinate y and reaches minimum value, after which it increases. The effect of dimensionless viscosity ratio β on the nanoparticles phenomena f as a function of y is illustrated in Fig. 14. It is found that in the interval of the normal coordinate $y \in [0.2, 0.45]$, i.e. near the lower-wall, the behavior of f for various values of β is exactly

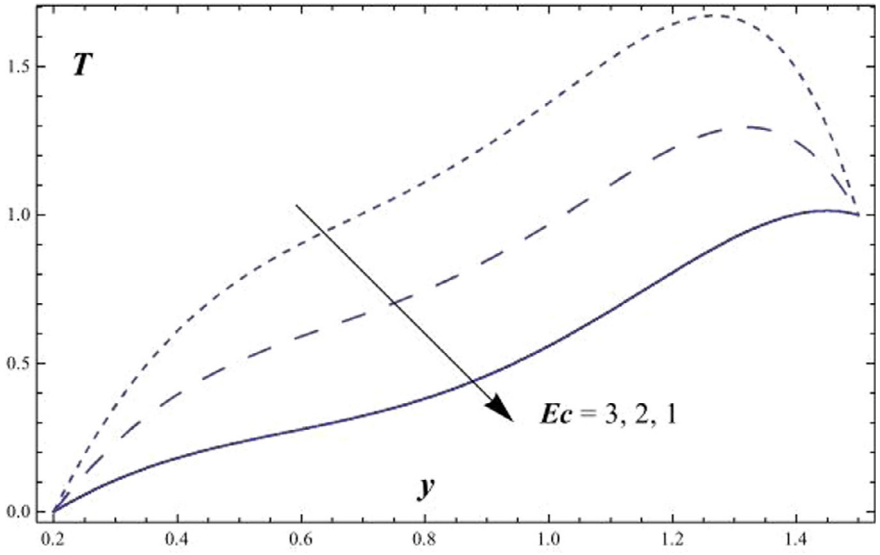

Fig. 8. The variation of temperature distribution versus y, with fixed $\beta = 0.5$, $\alpha = 1.2$, $\gamma = 2$, $\frac{dp}{dx} = -1$, Pr = 1, Re = 0.01, $N_b = 0.5$, $N_t = 1.5$, $R = 1$, $d = 0.8$, $a = 2$, $b = 1.8$, $\theta = \pi/2$, $x = 0.5$ for various values of Ec.

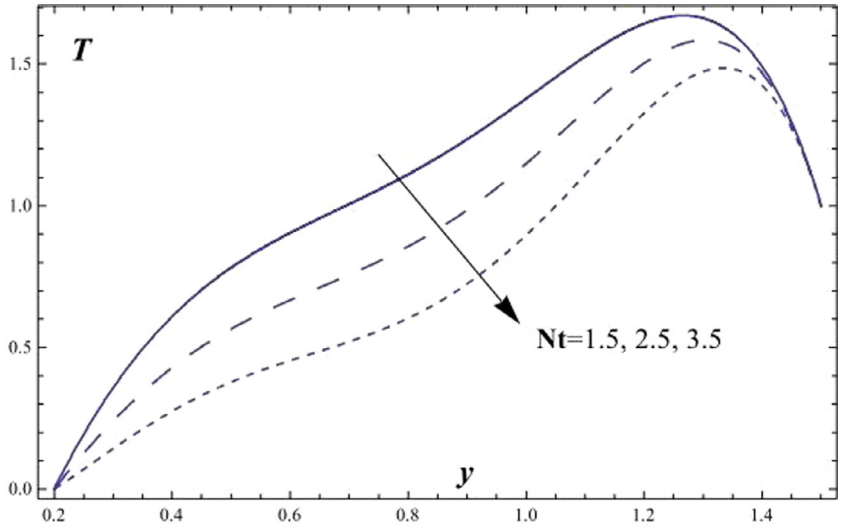

Fig. 9. The variation of temperature distribution versus y, with fixed $\beta = 0.5$, $\alpha = 1.2$, $Ec = 3$, $\gamma = 2$, $\frac{dp}{dx} = -1$, Pr = 1, Re = 0.01, $N_b = 0.5$, $R = 1$, $d = 0.8$, $a = 2$, $b = 1.8$, $\theta = \pi/2$, $x = 0.5$ for various values of N_t.

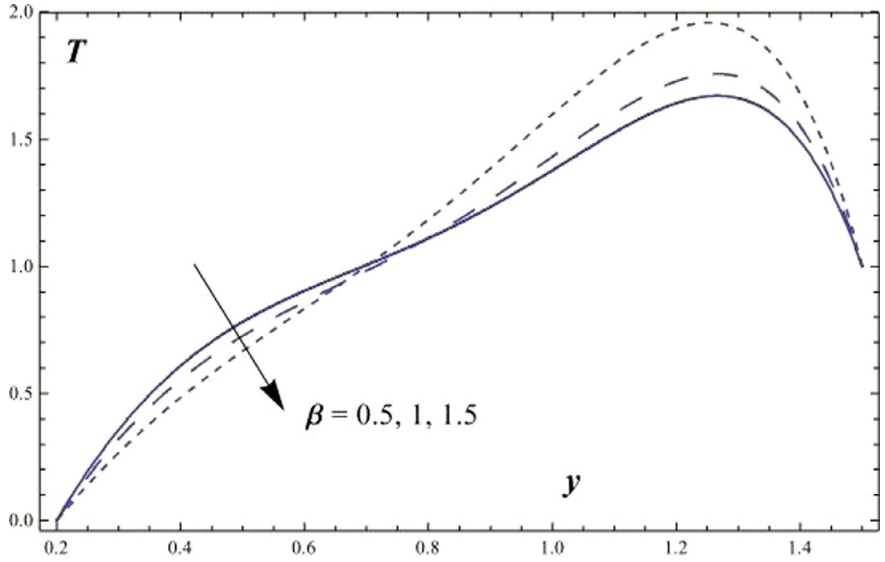

Fig. 10. The variation of temperature distribution versus y, with fixed $\alpha = 1.2$, $Ec = 3$, $\gamma = 2$, $\frac{dp}{dx} = -1$, Pr = 1, Re = 0.01, $N_b = 0.5$, $N_t = 1.5$, $R = 1$, $d = 0.8$, $a = 2$, $b = 1.8$, $\theta = \pi/2$, $x = 0.5$ for various values of β.

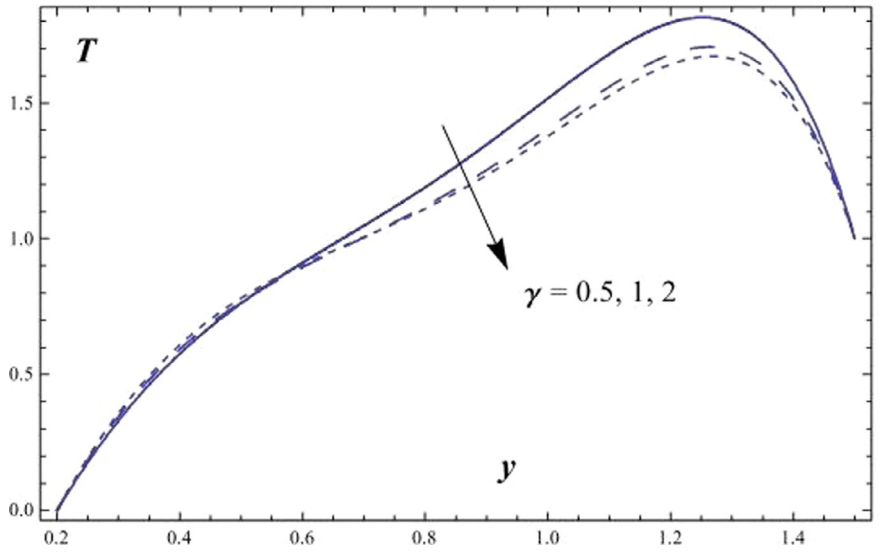

Fig. 11. The variation of temperature distribution versus y, with fixed $\beta = 0.5$, $\alpha = 1.2$, $Ec = 3$, $\frac{dp}{dx} = -1$, Pr = 1, Re = 0.01, $N_b = 0.5$, $N_t = 1.5$, $R = 1$, $d = 0.8$, $a = 2$, $b = 1.8$, $\theta = \pi/2$, $x = 0.5$ for various values of γ.

similar to the behavior of f for various values of N_b given in Fig. 12. It is also noted, from Fig. 14 that in the interval of the normal coordinate $y \in [0.2, 0.45]$, the behavior of f is an inversed manner of its behavior in the interval $y \in [0.45, 1.5]$ except that the curves are very close to each other in the first interval. In this case, for any value of the parameter β, there is a minimum value of f that holds at $y = 0.5$, and this minimal value slightly decreases by increasing the value of β . The effects of the other parameters are found to be similar to them; these figures are excluded here to avoid any kind of repetition.

Figs. 15 and 16 show the influence of β and γ on the shear stress τ_{xy} versus the parallel axis to wave propagation x. It is observed that the shear stress is smaller near the beginning and ending of the wave but becomes larger in the middle region, namely $x \in [0.2, 0.8]$. Fig. 15(i) and (ii) show that at the lower and upper walls, respectively, the shear stress decreases in the middle region, namely $x \in [0.2, 0.7]$, otherwise it increases, i.e. it increases in the first part and the last part of the wave. However, Fig. 16 (i) and (ii) depict that shear stress decreases in the first and last parts of the wave, whereas, it increases in the middle part of wave, namely $x \in [0.2, 0.7]$.

In Figs. 17–19, the behaviors of Nusselt number Nu with the parallel coordinate x, for various values of β, Ec and R at both lower and upper walls are presented respectively. It is noted in all figures that there is an oscillatory behavior between Nusselt number and x-axis which is due to the propagation of peristaltic waves along the walls of the channel. It is observed from Fig. 17(i) and (ii) that an increase of β increases Nusselt number near the beginning and ending of the wave, but it decreases in the central region, namely $x \in [0.2, 0.7]$. Fig. 18(i) and (ii), show that as Ec increases, Nusselt number increases at the lower wall, while it decreases at upper wall. Also, Nusselt number is plotted versus the coordinate x for various values of the power-law exponent m. It is clear from Fig. 19(i) and (ii), that the effect of R on Nu will behave in an

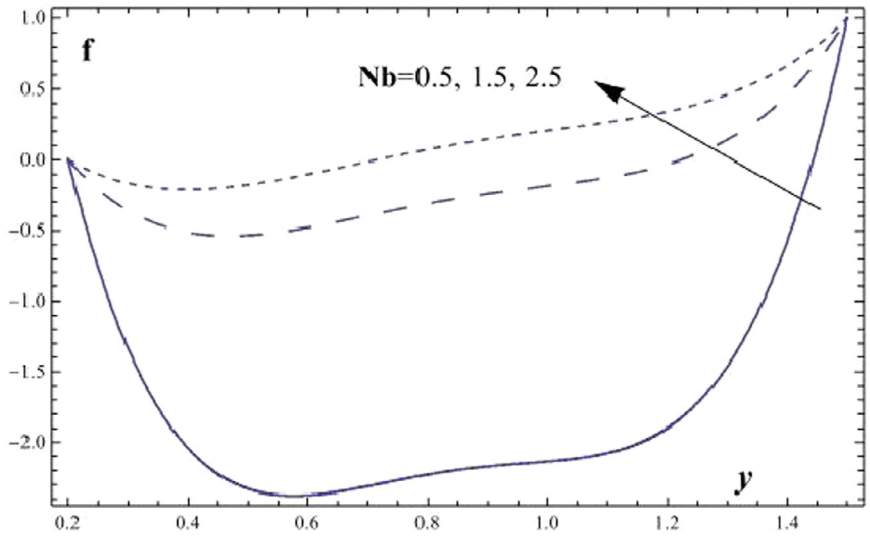

Fig. 12. The variation of nanoparticles phenomena versus y, with fixed $\beta = 0.5$, $\alpha = 1.2$, $Ec = 3$, $\gamma = 2$, $\frac{dP}{dx} = -1$, Pr = 1, Re = 0.01, $N_t = 1.5$, $R = 1$, $d = 0.8$, $a = 2$, $b = 1.8$, $\theta = \pi/2$, $x = 0.5$ for various values of N_b.

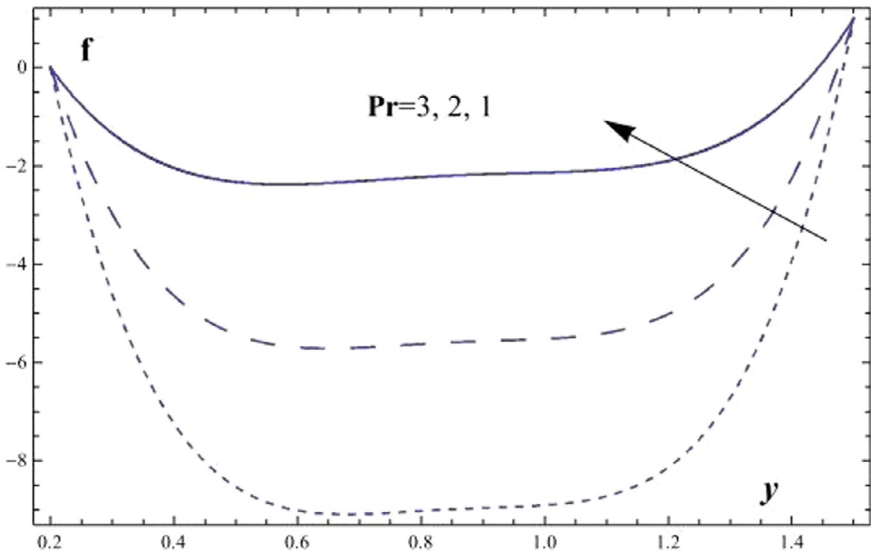

Fig. 13. The variation of nanoparticles phenomena versus y, with fixed $\beta = 0.5$, $\alpha = 1.2$, $Ec = 3$, $\gamma = 2$, $\frac{dP}{dx} = -1$, Re = 0.01, $N_b = 0.5$, $N_t = 1.5$, $R = 1$, $d = 0.8$, $a = 2$, $b = 1.8$, $\theta = \pi/2$, $x = 0.5$ for various values of Pr.

opposite manner to the effect of *Ec* on *Nu* that is given in Fig. 18 (i) and (ii) at both lower and upper walls.

Figs. 20i, ii, 21i, ii, 22i, and ii, portray the influence of β, Pr and Re on Sherwood number *Sh* versus *x*-axis at both lower and upper walls respectively. It is clearly observed that Sherwood number behaves at the lower (upper) wall in a similar manner as Nusselt number at the upper (lower) wall. Also the effect of β is to increase (decrease) *Sh* at both lower and upper walls. Also, the effect of Re and Pr on *Sh* at both lower and upper walls is similar to the effect of *Ec* and *R* on *Nu* that is given in Figs. 18 and 19.

Conclusion

This study extends the work of Mehmood et al. [19] in the case of zero order. The micropolar property, nanofluid and radiation effects weren't taken into their consideration. Because of the wide range of practical importance of the micropolar property, and nanofluid, the present study considered the effects of viscous dissipation on non-linear peristaltic mechanism with heat transfer of an incompressible micropolar non-Newtonian nanofluid in an asymmetric channel. The closed solutions of fluid velocity and microrotation velocity are obtained, and the solutions for temperature and nanoparticle profiles are obtained by using the homotopy perturbation method (HPM). The effects of various physical parameters acting on the problem such as micropolar, non-Newtonian, nanofluid, heat transfer, viscous dissipation, and radiation parameters are discussed through numerical computations and depicted graphically. The obtained results can be outlined and summarized as follows.

1. By increasing each of α, *Ec*, and Pr, the temperature increases while it decreases as *R*, *Re*, N_b, and N_t increases.
2. The temperature for different values of *Ec*, Pr, *Re*, N_b, and N_t becomes greater with increasing the normal-axis y and reaches the maximum value at $y \approx 1.2$.
3. The nanoparticles phenomena has an opposite behavior compared to temperature behavior except that it increases with the increase of γ, while the temperature increases (decreases).

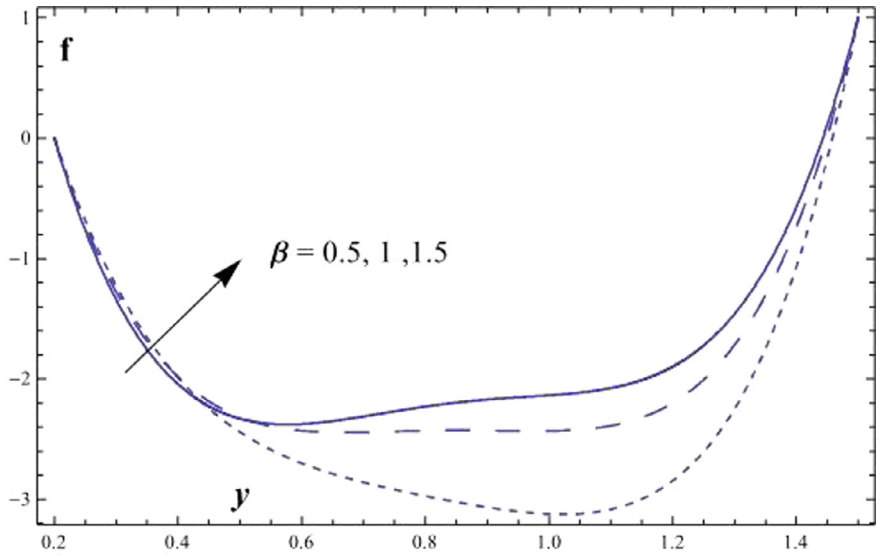

Fig. 14. The variation of nanoparticles phenomena versus y, with fixed $\alpha = 1.2$, $Ec = 3$, $\gamma = 2$, $\frac{dP}{dx} = -1$, Pr = 1, Re = 0.01, $N_b = 0.5$, $N_t = 1.5$, $R = 1$, $d = 0.8$, $a = 2$, $b = 1.8$, $\theta = \pi/2$, $x = 0.5$ for various values of β.

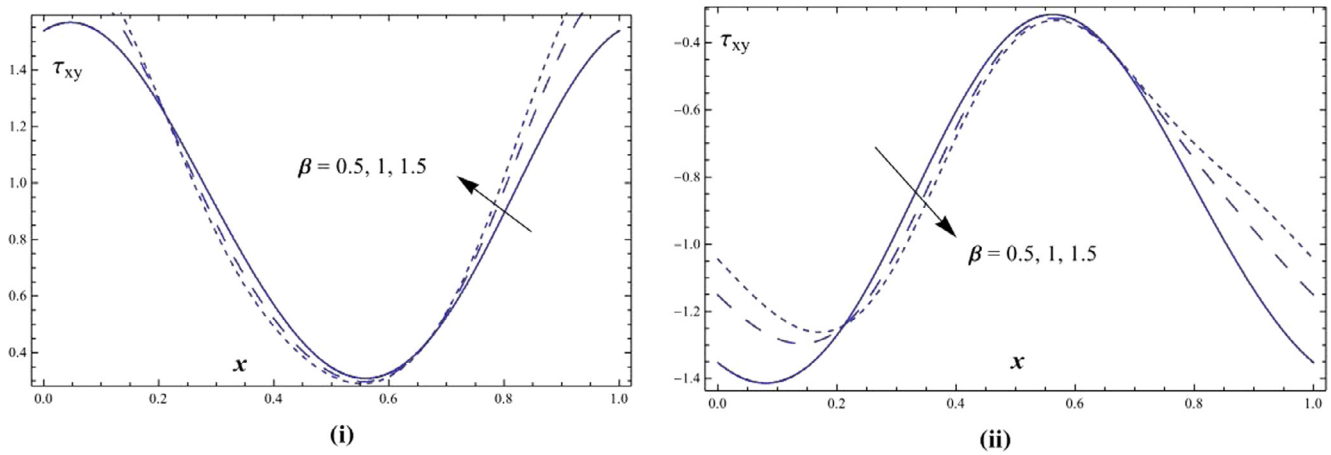

Fig. 15. (i), (ii) The variation of shear stress at both lower and upper walls versus x, with fixed $\alpha = 1.2$, $Ec = 3$, $\gamma = 2$, $\frac{dP}{dx} = -1$, Pr = 1, Re = 0.01, $N_b = 0.5$, $N_t = 1.5$, $R = 1$, $d = 0.8$, $a = 2$, $b = 1.8$, $\theta = \pi/2$ for various values of β.

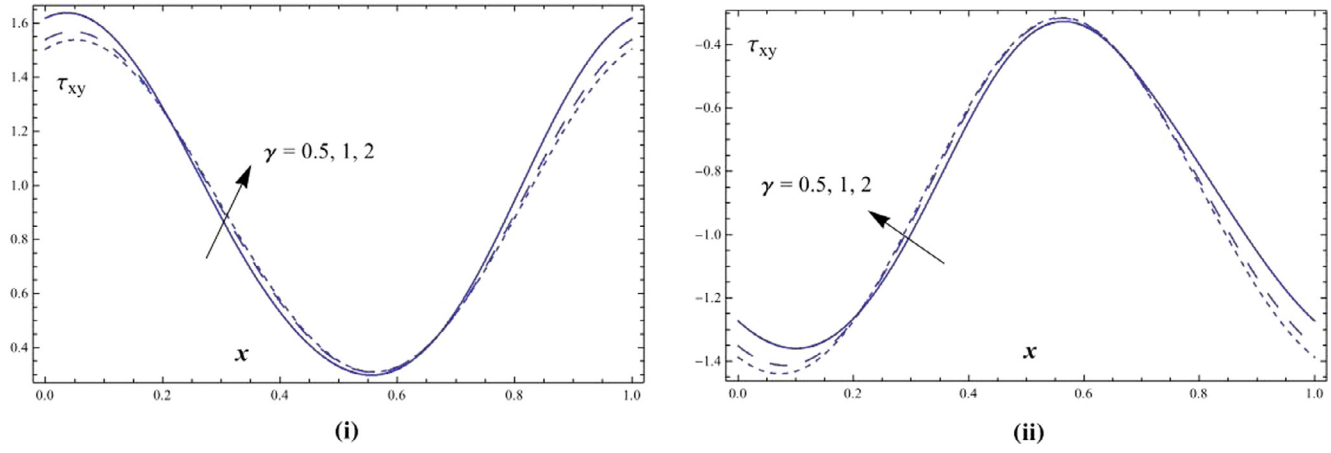

Fig. 16. (i), (ii) The variation of shear stress at both lower and upper walls versus x, with fixed $\beta = 0.5$, $\alpha = 1.2$, $Ec = 3$, $\frac{dP}{dx} = -1$, Pr = 1, Re = 0.01, $N_b = 0.5$, $N_t = 1.5$, $R = 1$, $d = 0.8$, $a = 2$, $b = 1.8$, $\theta = \pi/2$ for various values of γ.

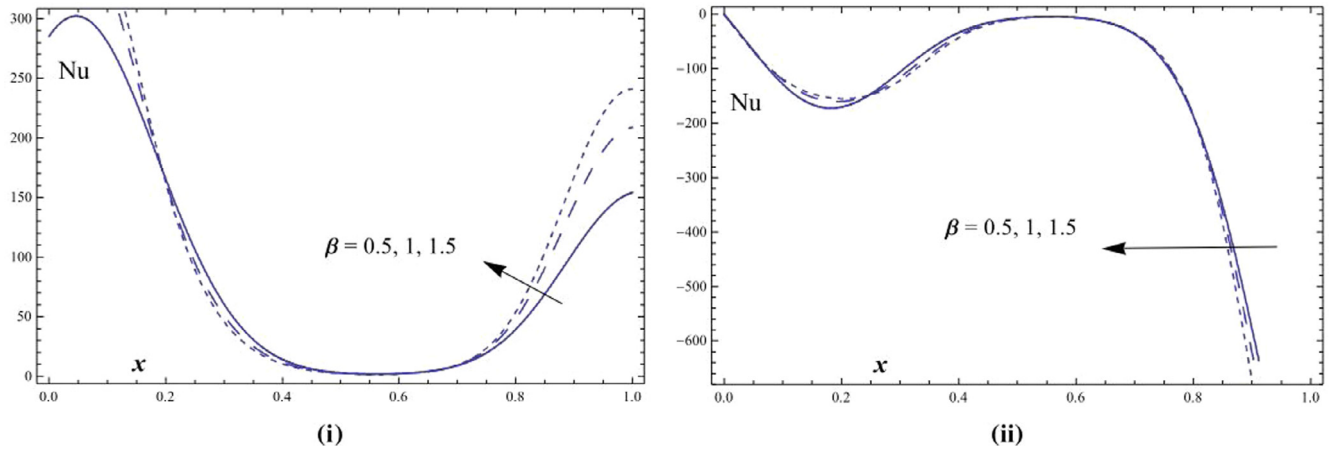

Fig. 17. (i), (ii) The variation of Nusselt number at both lower and upper walls versus x, with fixed $\alpha = 1.2$, $Ec = 3$, $\gamma = 2$, $\frac{dP}{dx} = -1$, Pr = 1, Re = 0.01, $N_b = 0.5$, $N_t = 1.5$, $R = 1$, $d = 0.8$, $a = 2$, $b = 1.8$, $\theta = \pi/2$ for various values of β.

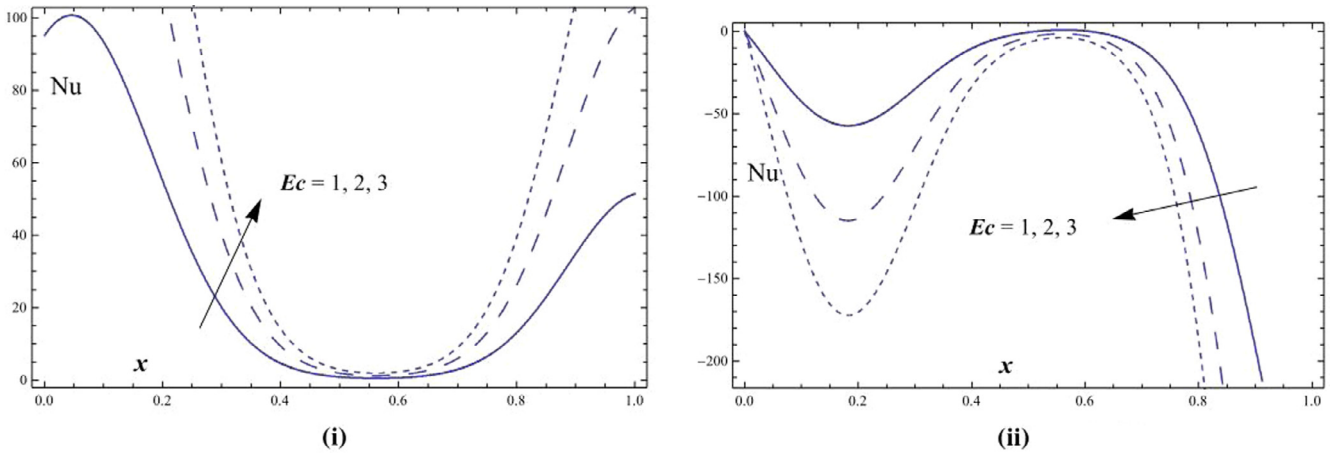

Fig. 18. (i), (ii) The variation of Nusselt number at both lower and upper walls versus x, with fixed $\beta = 0.5$, $\alpha = 1.2$, $\gamma = 2$, $\frac{dP}{dx} = -1$, Pr = 1, Re = 0.01, $N_b = 0.5$, $N_t = 1.5$, $R = 1$, $d = 0.8$, $a = 2$, $b = 1.8$, $\theta = \pi/2$ for various values of Ec.

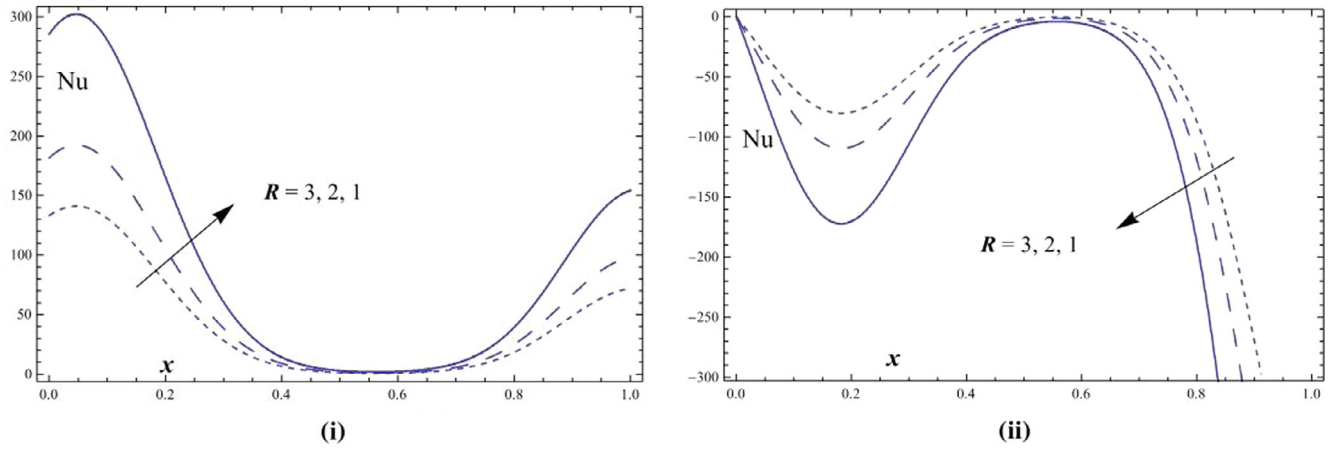

Fig. 19. (i), (ii) The variation of Nusselt number at both lower and upper walls versus x, with fixed $\beta = 0.5$, $\alpha = 1.2$, $Ec = 3$, $\gamma = 2$, $\frac{dP}{dx} = -1$, Pr = 1, Re = 0.01, $N_b = 0.5$, $N_t = 1.5$, $d = 0.8$, $a = 2$, $b = 1.8$, $\theta = \pi/2$ for various values of R.

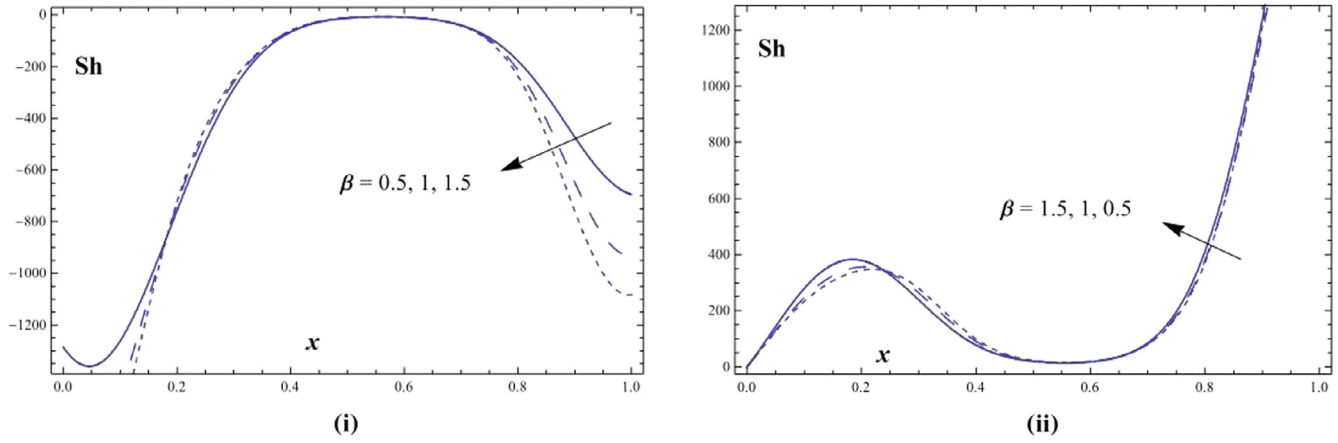

Fig. 20. (i), (ii) The variation of Sherwood number at both lower and upper walls versus x, with fixed $\alpha = 1.2$, $Ec = 3$, $\gamma = 2$, $\frac{dP}{dx} = -1$, Pr = 1, Re = 0.01, $N_b = 0.5$, $N_t = 1.5$, $R = 1$, $d = 0.8$, $a = 2$, $b = 1.8$, $\theta = \pi/2$ for various values of β.

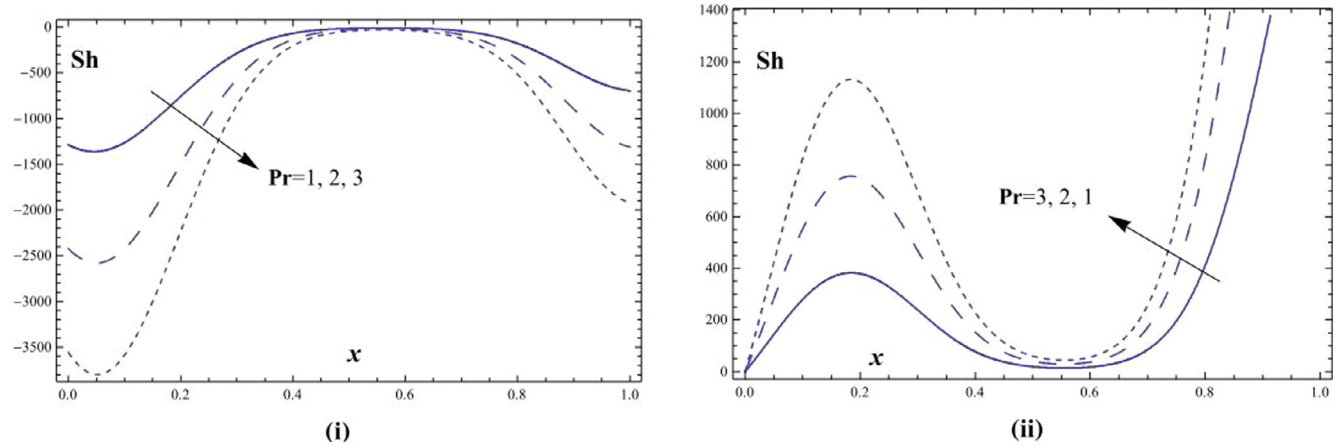

Fig. 21. (i), (ii) The variation of Sherwood number at both lower and upper walls versus x, with fixed $\beta = 0.5$, $\alpha = 1.2$, $Ec = 3$, $\gamma = 2$, $\frac{dP}{dx} = -1$, Re = 0.01, $N_b = 0.5$, $N_t = 1.5$, $R = 1$, $d = 0.8$, $a = 2$, $b = 1.8$, $\theta = \pi/2$ for various values of Pr.

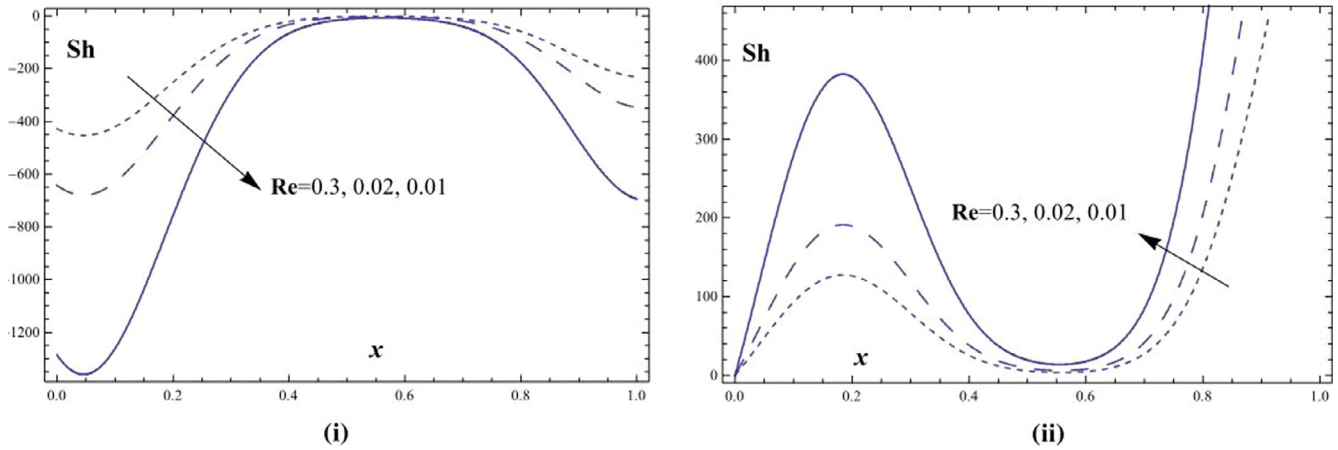

Fig. 22. (i), (ii) The variation of Sherwood number at both lower and upper walls versus x, with fixed $\beta = 0.5$, $\alpha = 1.2$, $Ec = 3$, $\gamma = 2$, $\frac{dP}{dx} = -1$, Pr = 1, $N_b = 0.5$, $N_t = 1.5$, $R = 1$, $d = 0.8$, $a = 2$, $b = 1.8$, $\theta = \pi/2$ for various values of Re.

4. The velocity u (increases) decreases with the increase in each of β and γ, and it increases as α and $\frac{dP}{dx}$ increase.
5. The velocity u for different values of β, γ, α and $\frac{dP}{dx}$ becomes greater with increasing y-axis and reaches a maximum value (at a finite value of y: $y = y_0$) after which it decreases.
6. The microrotation N decreases with the increase in each of β, α and $\frac{dP}{dx}$, whereas it decreases as γ increases.
7. The microrotation N is always negative and there is an inverse relation between N and y when $0 \leqslant y \leqslant 0.9$, otherwise, it increases as y increases.

8. For any values of x, at the beginning of the wave, $(\tau)_{h1}$, $(Nu)_{h1}$ and $(Sh)_{h2}$ decrease, while $(\tau)_{h2}$, $(Nu)_{h2}$ and $(Sh)_{h1}$ will behave in an opposite manner to the first behavior.

Appendix A

The constants a_1–a_{61} are given by

$$a_1 = \frac{\beta_1(2-\beta_1)}{\gamma},$$

$$\beta_1 = \frac{\beta}{((1+\alpha^{-1})+\beta)},$$

$$a_2 = \frac{\beta_1}{\gamma},$$

$$a_3 = \frac{(-(h_1+h_2)P_1\beta_1)}{2\gamma},$$

$$P_1 = \frac{(dP/dx)}{((1+\alpha^{-1})+\beta)},$$

$$a_4 = -\frac{(a_3+a_2h_1)}{a_1},$$

$$a_5 = -\frac{(a_3+a_2h_2)}{a_1},$$

$$a_6 = -\frac{\left(a_4e^{\sqrt{a_1}h_1} - a_5e^{\sqrt{a_1}h_2}\right)}{\left(e^{2\sqrt{a_1}h_1} - e^{2\sqrt{a_1}h_2}\right)},$$

$$a_7 = -\frac{e^{\sqrt{a_1}(h_1+h_2)}\left(a_5e^{\sqrt{a_1}h_1} - a_4e^{\sqrt{a_1}h_2}\right)}{\left(e^{2\sqrt{a_1}h_1} - e^{2\sqrt{a_1}h_2}\right)},$$

$$a_8 = e^{2\sqrt{a_1}h_1} - e^{2\sqrt{a_1}h_2},$$

$$a_9 = \frac{a_4}{a_8},$$

$$a_{10} = \frac{a_5}{a_8},$$

$$a_{11} = \frac{\sqrt{a_1}\left(a_{14}\left(e^{-\sqrt{a_1}h_2} - e^{-\sqrt{a_1}h_1}\right) + a_{13}\left(e^{\sqrt{a_1}h_1} - e^{-\sqrt{a_1}h_2}\right)\right)}{2(h_1-h_2)},$$

$$a_{12} = \frac{(\beta_1a_2 + P_1a_1)}{6a_1},$$

$$a_{13} = -\frac{\beta_1a_6}{a_1},$$

$$a_{14} = -\frac{\beta_1a_7}{a_1},$$

$$a_{15} = -\frac{\left((-1+\sqrt{a_1}(a_{14}e^{-\sqrt{a_1}h_1} - a_{13}e^{\sqrt{a_1}h_1}))h_2 - 3a_{12}h_1^2h_2 + h_1\left(1+\sqrt{a_1}(a_{13}e^{\sqrt{a_1}h_2} - a_{14}e^{-\sqrt{a_1}h_2}) + 3a_{12}h_2^2\right)\right)}{h_1-h_2},$$

$$\begin{aligned} a_{16} = {} & e^{-\sqrt{a_1}(h_1+h_2)}\Big(a_{14}\Big(-\sqrt{a_1}e^{\sqrt{a_1}h_1}h_1^2 + e^{\sqrt{a_1}h_2} \\ & \times\Big(-\sqrt{a_1}h_1^2 + 2h_2 + 2h_1(-1+\sqrt{a_1}h_2)\Big)\Big) \\ & + e^{\sqrt{a_1}(h_1+h_2)}(h_1(2+a_{12}h_1(h_1-3h_2))(h_1-h_2) \\ & + a_{13}\Big(\sqrt{a_1}e^{\sqrt{a_1}h_2}h_1^2 + e^{\sqrt{a_1}h_1}\Big(\sqrt{a_1}h_1^2 + 2h_2 - 2h_1\left(1+\sqrt{a_1}h_2\right)\Big)\Big)\Big)\Big) \\ & /2(h_1-h_2), \end{aligned}$$

$$a_{17} = -\frac{a_{13}e^{\sqrt{a_1}h_1} + a_{14}e^{-\sqrt{a_1}h_1} + h_1^2(a_{11}+a_{12}h_1)}{h_1},$$

$$a_{18} = \frac{a_{17}h_2}{h_1-h_2},$$

$$a_{19} = h_1\Big(a_{13}e^{\sqrt{a_1}h_2} + a_{14}e^{-\sqrt{a_1}h_2} + h_2^2(a_{11}+a_{12}h_2)\Big),$$

$$a_{20} = \frac{6Ec}{\mathrm{Re}(3+4R)},$$

$$a_{21} = \frac{a_{22}(N_b+2N_t)}{2\sqrt{a_1}(h_1-h_2)},$$

$$a_{22} = -\frac{a_{20}(a_1a_{14}a_7\beta_1 + a_7^2\beta_1 + a_1^2a_{14}^2\mathrm{Pr})}{4a_1}$$

$$\begin{aligned} a_{23} = {} & a_{20}\Big(4a_2a_7\beta_1 + 2\sqrt{a_1}a_3a_7\beta_1 + \sqrt{a_1^3}(a_{14}a_3 - 2a_{11}a_7)\beta_1 \\ & + 2a_1(a_2a_{14} - 6a_{12}a_7)\beta_1 - 4\sqrt{a_1^5}a_{11}a_{14}\mathrm{Pr} - 24a_1^2a_{12}a_{14}\mathrm{Pr}\Big)\Big/\sqrt{a_1^5}, \end{aligned}$$

$$a_{24} = a_{20}(2a_2a_7\beta_1 + a_1(a_{14}a_2 - 6a_{12}a_7)\beta_1 - 12a_1^2a_{12}a_{14}\mathrm{Pr})/a_1^2$$

$$\begin{aligned} a_{27} = {} & a_{20}\Big(-4a_2a_6\beta_1 + 2\sqrt{a_1}a_3a_6\beta_1 + \sqrt{a_1^3}(a_{13}a_3 - 2a_{11}a_6)\beta_1 \\ & - 2a_1(a_2a_{13} - 6a_{12}a_6)\beta_1 - 4\sqrt{a_1^5}a_{11}a_{13}\mathrm{Pr} + 24a_1^2a_{12}a_{13}\mathrm{Pr}\Big)\Big/\sqrt{a_1^5}, \end{aligned}$$

$$a_{28} = \frac{a_{20}(2a_2a_6\beta_1 + a_1(a_{13}a_2 - 6a_{12}a_6)\beta_1 - 12a_1^2a_{12}a_{13}\mathrm{Pr})}{a_1^2},$$

$$a_{31} = -\frac{a_{20}(a_1a_{13}a_6\beta_1 + a_6^2\beta_1 + a_1^2a_{13}^2\mathrm{Pr})}{4a_1},$$

$$\begin{aligned} a_{32} = {} & \frac{1}{2}\Big(\frac{2a_{20}a_{11}a_3\beta_1}{a_1} - \frac{a_{20}a_3^2\beta_1}{a_1^2} - a_1a_{20}(a_{14}a_6 - a_{13}a_7)\beta_1 \\ & - 2a_1^2a_{13}a_{14}a_{20}\mathrm{Pr} + \frac{N_b+N_t-2a_{20}(h_2-h_1)^2(a_6a_7\beta_1 + 2a_{11}^2\mathrm{Pr})}{(h_2-h_1)^2}\Big), \end{aligned}$$

$$a_{33} = \frac{a_{20}(-a_2a_3\beta_1 + a_1(a_{11}a_2 + 3a_{12}a_3)\beta_1 - 12a_1^2a_{11}a_{12}\mathrm{Pr})}{3a_1^2},$$

$$a_{34} = \frac{-a_{20}\left(-6a_1a_{12}\beta_1 + a_2^2\beta_1 + 36a_1^2a_{12}^2\mathrm{Pr}\right)}{12a_1^2},$$

$$a_{35} = a_{21} + a_{22},$$

$$a_{36} = a_{23} + a_{43},$$

$$a_{37} = a_{24} + a_{44},$$

$$a_{38} = a_{27} + a_{47},$$

$$\begin{aligned} a_{39} = -\frac{1}{h_1 - h_2}\big(&a_{22}e^{-2\sqrt{a_1}h_1} + a_{31}e^{2\sqrt{a_1}h_1} - a_{22}e^{-2\sqrt{a_1}h_2} - a_{31}e^{2\sqrt{a_1}h_2} \\ &+a_{32}h_1^2 + a_{33}h_1^3 + a_{34}h_1^4 + e^{-\sqrt{a_1}h_1}(a_{23} + a_{24}h_1) \\ &+e^{\sqrt{a_1}h_1}(a_{27} + a_{28}h_1) - a_{32}h_2^2 - a_{33}h_2^3 - a_{34}h_2^4 \\ &-e^{-\sqrt{a_1}h_2}(a_{23} + a_{24}h_2) - e^{\sqrt{a_1}h_2}(a_{27} + a_{28}h_1)\big), \end{aligned}$$

$$\begin{aligned} a_{40} = -\frac{1}{h_1 - h_2}\big(&a_{22}e^{-2\sqrt{a_1}h_2}h_1 + a_{23}e^{-\sqrt{a_1}h_2}h_1 + a_{27}e^{\sqrt{a_1}h_2}h_1 \\ &+a_{31}e^{2\sqrt{a_1}h_2}h_1 - a_{22}e^{-2\sqrt{a_1}h_1}h_2 - a_{23}e^{-\sqrt{a_1}h_1}h_2 - a_{27}e^{\sqrt{a_1}h_1}h_2 \\ &-a_{31}e^{2\sqrt{a_1}h_1}h_2 - a_{24}e^{-\sqrt{a_1}h_1}h_1h_2 - a_{28}e^{\sqrt{a_1}h_1}h_1h_2 \\ &+a_{24}e^{-\sqrt{a_1}h_2}h_1h_2 + a_{28}e^{\sqrt{a_1}h_2}h_1h_2 - a_{32}h_1^2h_2 - a_{33}h_1^3h_2 \\ &-a_{34}h_1^4h_2 + a_{32}h_1h_2^2 + a_{33}h_1h_2^3 + a_{34}h_1h_2^4\big), \end{aligned}$$

$$a_{43} = \frac{(\sqrt{a_1}a_{23} + a_{24})(N_b + 2N_t)}{a_1(h_1 - h_2)},$$

$$a_{44} = \frac{a_{24}(N_b + 2N_t)}{\sqrt{a_1}(h_1 - h_2)},$$

$$a_{45} = a_{28} + a_{48},$$

$$a_{46} = a_{31} + a_{51},$$

$$a_{47} = \frac{(\sqrt{a_1}a_{27} - a_{28})(N_b + 2N_t)}{a_1(h_1 - h_2)},$$

$$a_{48} = -\frac{a_{28}(N_b + 2N_t)}{\sqrt{a_1}(h_1 - h_2)},$$

$$a_{50} = a_{34} + a_{54},$$

$$a_{51} = -\frac{a_{31}(N_b + 2N_t)}{2\sqrt{a_1}(h_1 - h_2)},$$

$$a_{52} = \frac{N_b^2 - (a_{39} + a_{41})N_bN_t(h_1 - h_2) - 2a_{39}(h_1 - h_2)N_t^2}{2(h_1 - h_2)^2N_t},$$

$$a_{53} = -\frac{a_{32}(N_b + 2N_t)}{3(h_1 - h_2)},$$

$$a_{54} = -\frac{a_{33}(N_b + 2N_t)}{4(h_1 - h_2)},$$

$$a_{55} = -\frac{a_{34}(N_b + 2N_t)}{5(h_1 - h_2)},$$

$$a_{56} = a_{33} + a_{53},$$

$$a_{57} = a_{32} + a_{52},$$

$$a_{58} = a_{39} + a_{60},$$

$$a_{59} = a_{40} + a_{61},$$

$$\begin{aligned} a_{60} = &\frac{e^{-2\sqrt{a_1}(h_1+h_2)}}{2(h_1 - h_2)^3N_t}\Big(2(h_1 - h_2)^2N_t\big(a_{21}e^{2\sqrt{a_1}h_1} - a_{21}e^{2\sqrt{a_1}h_2} \\ &-a_{51}e^{2\sqrt{a_1}(2h_1+h_2)} + a_{51}e^{2\sqrt{a_1}(h_1+2h_2)}\big) \\ &-2e^{\sqrt{a_1}(h_1+2h_2)}(h_1 - h_2)^2(a_{43} + a_{44}h_1)N_t \\ &-2e^{\sqrt{a_1}(3h_1+2h_2)}(h_1 - h_2)^2(a_{47} + a_{48}h_1)N_t \\ &+2e^{\sqrt{a_1}(2h_1+h_2)}(h_1 - h_2)^2(a_{43} + a_{44}h_2)N_t \\ &+2e^{\sqrt{a_1}(2h_1+3h_2)}(h_1 - h_2)^2(a_{47} + a_{48}h_2)N_t \\ &+e^{2\sqrt{a_1}(h_1+h_2)}\Big(-2a_{53}(h_1 - h_2)^2h_1^3N_t - 2a_{54}(h_1 - h_2)^2h_1^4N_t \\ &-2a_{55}(h_1 - h_2)^2h_1^5N_t + h_1^2(-N_b^2 + (a_{39} + a_{41})(h_1 - h_2)N_tN_b \\ &+2a_{39}(h_1 - h_2)N_t^2) + h_2^2\Big(N_b^2 - (a_{39} + a_{41})(h_1 - h_2)N_tN_b \\ &+2(h_1 - h_2)N_t\Big(a_{35}(h_1 - h_2)h_2 + a_{54}(h_1 - h_2)h_2^2 + a_{55}(h_1 - h_2)h_2^3 - a_{39}N_t\Big)\Big)\Big)\Big), \end{aligned}$$

$$\begin{aligned} a_{61} = \frac{-1}{(h_1 - h_2)}\Bigg(&h_1\Bigg(a_{21}e^{-2\sqrt{a_1}h_2} + a_{51}e^{2\sqrt{a_1}h_2} + a_{53}h_2^3 + a_{54}h_2^4 \\ &+a_{55}h_2^5 + e^{-\sqrt{a_1}h_2}(a_{43} + a_{44}h_2) + e^{\sqrt{a_1}h_2}(a_{47} + a_{48}h_2) \\ &+\frac{h_2^2(N_b^2 - (a_{39} + a_{41})h_1 - h_2)N_tN_b - 2a_{39}(h_1 - h_2)N_t^2)}{2(h_1 - h_2)^2N_t}\Bigg) \\ &+h_2\Bigg(-a_{21}e^{-2\sqrt{a_1}h_1} - a_{51}e^{2\sqrt{a_1}h_1} - a_{53}h_1^3 - a_{54}h_1^4 - a_{55}h_1^5 \\ &-e^{-\sqrt{a_1}h_1}(a_{43} + a_{44}h_1) - e^{\sqrt{a_1}h_1}(a_{47} + a_{48}h_1) \\ &+\frac{h_1^2(-N_b^2 + (a_{39} + a_{41})(h_1 - h_2)N_tN_b + 2a_{39}(h_1 - h_2)N_t^2)}{2(h_1 - h_2)^2N_t}\Bigg)\Bigg). \end{aligned}$$

References

[1] Nadeem S, Maraj EN, Sher Akbar N. Investigation of peristaltic flow of Williamson nanofluid in a curved channel with compliant walls. Appl Nanosci 2014;4:511–21.

[2] Estellé P, Halelfadl S, Doner N, Maré T. Shear history effect on the viscosity of carbon nanotubes water-based nanofluid. Curr Nanosci 2013;9:225–30.

[3] Saeed ZH, Seyyed HN, Elham T, Javad S. Numerical investigation of Al_2O_3/water nanofluid laminar convective heat transfer through triangular ducts. Nanoscale Res Lett 2011;8:179–88.

[4] Mustafaa M, Hina S, Hayat T, Alsaedi A. Influence of wall properties on the peristaltic flow of a nanofluid: analytic and numerical solutions. Int J Heat Mass Transfer 2012;55:4871–7.

[5] Umavathi JC, Shekar M. Effect of MHD on Jeffery-Hamel flow in nanofluids by differential transform method. Int J Eng Res Appl 2013;3:953–62.

[6] Khan MS, Karim I, Ali LE, Islam A. Unsteady MHD free convection boundary-layer flow of a nanofluid along a stretching sheet with thermal radiation and viscous dissipation effects. Int Nano Lett 2012;2:24. http://dx.doi.org/10.1186/2228-5326-2-24.

[7] Eringen AC. Theory of thermomicrofluids. J Math Anal Appl 1972;38:480–96.

[8] Agrawal RS, Dhanapal C. Numerical solution to the flow of a micropolar fluid between porous walls of different permeability. Int J Eng Sci 1987;25:325–36.

[9] Nadeem S, Rehman A, Vajravelu K, Lee J, Lee C. Axisymmetric stagnation flow of a micropolar nanofluid in a moving cylinder. Math Prob Eng 2012:1–18. ID 378259.

[10] Muth P, Rathish kumar BV, Chandra P. Peristaltic flow of a micropolar fluid in an asymmetric channel. ANZIAM J 2003;45:245–60.

[11] Ali N, Hayat T. Peristaltic flow of a micropolar fluid in an asymmetric channel. Comput Math Appl 2008;55:589–608.

[12] Abd Elmaboud Y. Thermomicropolar fluid flow in a porous channel with peristalsis. J Porous Media 2011;14:1033–45.

[13] Eldabe NT, Abou-zeid MY. Magnetohydrodynamic peristaltic flow with heat and mass transfer of micropolar biviscosity fluid through a porous medium between two co-axial tubes. Arab J Sci Eng 2014;39:5045–62.

[14] Eldabe NT, Abou-zeid MY. The wall properties effect on peristaltic transport of micropolar non-Newtonian fluid with heat and mass transfer. Math Prob Eng 2010:1–40. ID 898062.

[15] Ferdows M, Olajuwon BI. On the similarity solution of micropolar power-law fluid over a vertical plate. Int J Contemp Math Sci 2011;6:133–43.

[16] Wang C. Unique solvability for the non-Newtonian magneto-micropolar fluid. Boundary Value Prob 2013;2013:182.

[17] Ellahi R, Rahman SU, Mudassar Gulzar M, Nadeem S, Vafai K. A mathematical study of non-Newtonian micropolar fluid in arterial blood flow through composite stenosis. Appl Math Inf Sci 2014;8:1567–73.

[18] Haile E, Shankar B. Heat and mass transfer through a porous media of MHD flow of nanofluids with thermal radiation, viscous dissipation and chemical reaction effects. Am Chem Sci J 2014;4:828–46.
[19] Mehmood OU, Mustapha N, Shafie S. Nonlinear peristaltic flow of Walter's b fluid in an asymmetric channel with heat transfer and chemical reactions. Therm Sci doi:10.2298/TSCI110921096M.
[20] Wilson SDR, Taylor AJ. The channel entry problem for a yield stress fluid. J Non-Newtonian Fluid Mech 1996;65:165–76.
[21] Ahmadi G. Self-similar solution of incompressible micropolar boundary layer flow over a semi-infinite plate. Int J Eng Sci 1976;14:639–46.
[22] Rohsenow WM, Hartnett JP, Cho YI. Handbook of heat transfer. New York: McGraw-Hill; 1998.
[23] Anbuchezhian N, Srinivasan K, Chandrasekaran K, Kandasamy R. Thermophoresis and Brownian motion effects on boundary layer flow of nanofluid in presence of thermal stratification due to solar energy. Appl Math Mech Engl Ed 2012;33:765–80.
[24] Shaaban AA. Numerical solutions of some problems in biomechanics and its applications in the human body Ph.D. thesis. Cairo, Egypt: Ain Shams University; 2007.
[25] Ravi YVK, Kumar YVK, Krishna Kumari SVHN, Ramana Murthy MV, Sreenadh S. Peristaltic transport of a power-law fluid in an asymmetric channel bounded by permeable walls. Adv Appl Sci Res 2011;2:396–406.
[26] Nowar Kh. Peristaltic flow of a nanofluid under the effect of hall current and porous medium. Math Probl Eng 2014:1–15. ID 389581.